Study on the Permeability and Mechanical Properties of Copper Powder/Mesh Porous Plates

YINGMAO CHEN[1] and ZHAOYAO ZHOU[1,2]

1.—Guangdong Key Laboratory for Processing and Forming of Advanced Metallic Materials, School of Mechanical and Automotive Engineering, South China University of Technology, Guangzhou 510640, China. 2.—e-mail: zhyzhou@scut.edu.cn

Copper powder and copper wire mesh were used as raw materials, and porous copper powder/mesh plates were prepared by pressing, rolling, and vacuum sintering. The plate morphology was observed by scanning electron microscopy. The air permeability of the porous plates was tested according to Darcy's law, and uniaxial tensile tests were carried out on the porous plates to determine the influence of raw material mesh number and powder content on the porous plates' permeability and tensile mechanical properties. The porous plate was fabricated into a restrictor of an aerostatic thrust bearing, and the static bearing performance of the bearing was tested on a bearing capacity testing platform. The results showed that the copper powder/mesh porous plate had a uniform pore distribution and a porosity range of 10% to 30%; the higher the porosity and lower the powder concentration, the better the performance was in terms of gas permeability. Tensile mechanical properties improved with decreasing porosity and increasing powder content. At a gas film thickness of 10 μm, the prepared gas hydrostatic thrust bearing could support a maximum load of 381.1 N.

INSTRUCTION

As a kind of metal porous material, metal powder/mesh porous material integrates the double advantages of powder metallurgy material with numerous pores and sieve material with high strength of continuous dense body, but the traditional process of manufacturing powder/mesh porous material still has the defects of complex manufacturing process and low mechanical properties, which seriously restrict the expansion of its application field.[1–4] With the metal powder/mesh porous materials from simple filtration function material to gas hydrostatic bearing porous throttle material for transformation, the material permeability and mechanical properties put forward higher requirements.[5–10]

Scholars at home and abroad have extensively researched porous materials' permeability and tensile properties. For example, Zhou et al.[11] studied the permeability of stainless steel wire mesh porous materials. They found that stainless steel wire mesh porous materials with more significant porosity and smaller thickness had a higher permeability. Mancin et al.[12] experimentally studied the pressure drop of compressed air passing through six aluminum open-cell foam materials with different pore numbers and porosity distributions ranging from 90.3% to 95.6%. The results showed that the pressure difference of compressed air before and after passing through the material increased with the increase of the compressed air flow rate, and the permeability coefficient of the material also increased with the increase of the average pore size and porosity of the material. Zou et al.[13] prepared copper powder microporous materials using spherical copper powder and copper metal fibers and investigated the tensile properties of the materials. The experimental results indicated that the tensile strength of the materials decreased with the increase of material porosity, increased with the increase of copper powder content, and increased with the increase of sintering temperature. Li et al.[14] prepared stainless steel powder/wire mesh composite sheets using stainless steel powder and
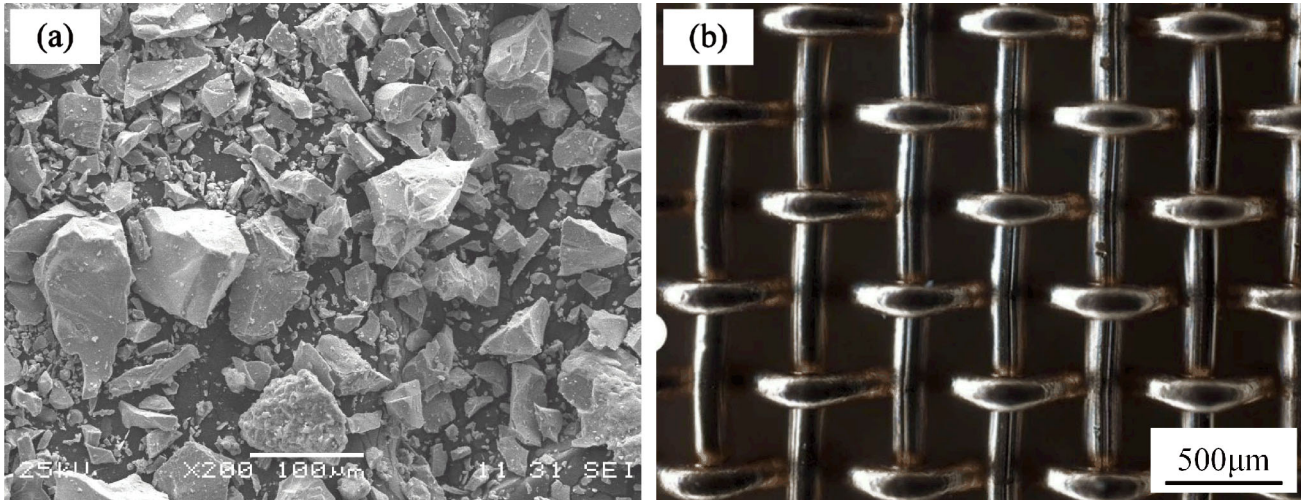
Fig. 1. Micrographs of the (a) copper powder and (b) copper wire mesh.

wire mesh and conducted a detailed study on the composite sheets' permeability and tensile mechanical properties. The results indicated that the simpler the structure of the gradient porous plate, the better its permeability. Among them, the air permeability of the wire mesh gradient porous plate prepared from three different wire diameters (3WMGPP) was 5.84×10^{-13} m^2. As the porosity decreased, the deformation-strengthening ability of gradient porous plates gradually increased, and the tensile strength significantly increased.

Compared with stainless steel wire mesh, copper wire mesh has better ductility and hydrophobicity and can adapt to the requirements of more fluid media when made into a porous throttling device. There are few reports on the permeability and mechanical properties of copper powder/wire mesh porous materials. Therefore, studying the influence of manufacturing process parameters on the permeability and mechanical properties of copper powder/wire mesh porous materials is of great importance for further improving the material properties.

MATERIALS AND METHODS

Material Preparation

The red copper plain wire mesh with purity of 99.95–99.99% produced by Anping County Hangying Wire Mesh was adopted as the copper wire mesh, and the irregular copper powder produced by Nangong Fufan Metal Materials Co., Ltd., to ensure the quality of powder during material rolling was selected as the copper powder. Figure 1 shows the morphology of the raw materials for copper wire mesh and copper powder.

In this work, 80 mesh, 150 mesh, and 200 mesh copper wire mesh and copper powder were used as raw materials. The wire diameter and pore size data of the wire mesh are shown in Table I. As the mesh

size increased, the wire diameter, pore size, and single-layer thickness of the copper wire mesh gradually decreased. The average diameter of the 80 mesh powder was 0.182 mm, the average diameter of the 150 mesh powder was 0.100 mm, and the average diameter of the 200 mesh powder was 0.075 mm.

The material preparation process is illustrated in Fig. 2. First, some copper wire mesh was cut into 100-mm-wide wire mesh strips as the substrate material for the wire mesh/powder rolling process, and the rest was cut into 100 mm × 100-mm wire mesh thin sheets. An ultrasonic vibration powder feeder was used to sieve the powder and roll the wire mesh and powder together to obtain the powder/wire mesh composite strip. Then, the wire mesh thin sheets and powder/wire mesh composite strips cut into 100 mm × 100 mm were stacked staggered to obtain a loose body. To achieve an interlayer composite, the loose body was made into a rigid whole. The resulting body was pressed by a large press with a pressing force of 300 t, followed by a large rolling mill with a rolling force of 240 t and a rolling speed of 340 mm/s for composite rolling. However, after rolling, the composite mechanism was only mechanical bonding without material diffusion and transfer, resulting in low strength. A small amount of deformation could cause the interlayer of the metal wire mesh to tear and the metal powder to fall off. Finally, to increase the bonding strength, the mechanical bonding inside the material was transformed into metallurgical bonding, and the material was vacuum sintered to obtain a porous composite material with a porous structure and a particular strength. The sintering temperature-time curve is shown in Fig. 3a.

A wire-cut processing method was used to obtain the required test specimens to protect the surface pores of porous materials. Before the performance

Table I. Eight kinds of powder/screen porous plate specification parameters

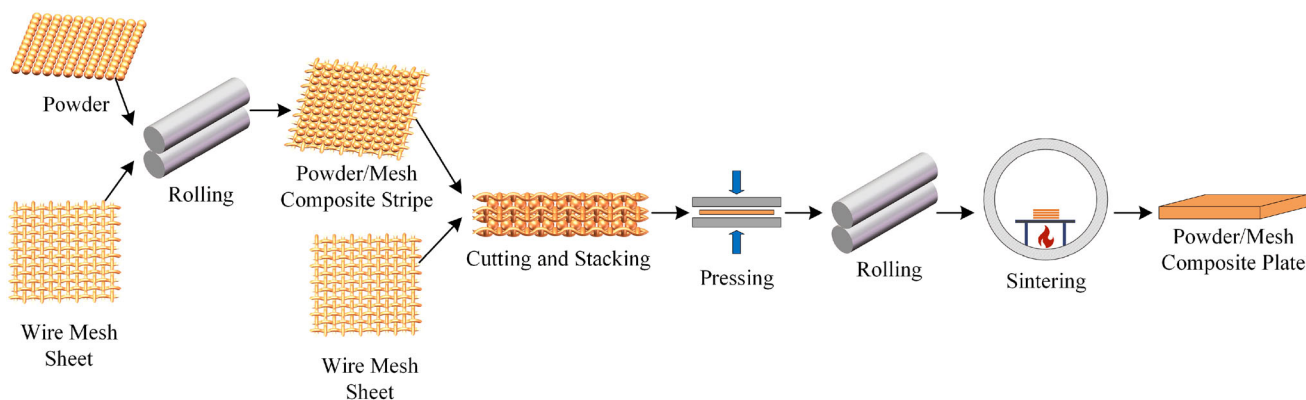| Sample	Mesh size	Powder content (%)	Sintering temperature (°C)	Porosity (%)
1	80	0	850	24.31
2	80	16.52	850	20.51
3	150	16.59	850	20.63
4	200	16.48	850	20.88
5	80	22.89	850	20.04
6	80	28.36	850	19.70
7	80	33.10	850	19.11
8	80	49.73	850	16.88

Fig. 2. Preparation process of copper powder/mesh porous plates.

test, the samples were cleaned and dried, and the porosity was calculated. Since the raw materials were all copper wire mesh and copper powder, and there were no inclusions of different densities, the mass volume method was used to calculate the sample porosity, as shown below directly:

$$P = \left(1 - \frac{m}{\rho V}\right) \times 100\% \qquad (1)$$

where P is the average porosity of the sample (%), m is the mass of the sample (g), V is the volume of the sample (cm^3), and ρ is the density of copper (8.96 g·cm^{-3}).

Air Permeability Test

The number of through-holes and blind holes in powder/wire mesh porous plates could not be determined by scanning electron microscopy and bubble pressure methods, so other indicators were used to evaluate the breathability of the porous plates.[15,16] A breathable performance sample with a diameter of 24 mm was cut from the porous plate, and then compressed clean air of 0.2 MPa, 0.4 MPa, and 0.6 MPa was passed through it. Finally, its pressure drop and volume flow rate were measured to evaluate the permeability coefficient using the Darcy-Forsyheimer formula, as shown below:

$$\frac{\Delta p}{L} = \frac{\mu}{K_1}v + \frac{\rho}{K_2}v^2 \qquad (2)$$

where Δp is the pressure difference between the two ends of the sample (Pa), L is the thickness of the sample (m), μ is the viscosity of the gas, the viscosity of air at room temperature is 17.9×10^{-6} Pa s, and ρ is the density of the gas; the density of air is 1.29 kg·m^3 at room temperature conditions. K_1 is the viscous permeability coefficient of the sample (m^2), and K_2 is the inertial permeability coefficient of the sample (m).

The flow resistance performance of fluid passing through metal wire mesh materials is evaluated by two coefficients: viscous permeability coefficient and inertial permeability coefficient. The primary evaluation basis is the viscous permeability coefficient K_1. The air permeability testing system used in the experiment is shown in Fig. 3b. Clean air flowed from the air compressor through a gas pipe to an air filter and then through an airflow meter to the sample room. After passing through the sample room, the pressure difference between the two ends was calculated and recorded by a pressure sensor connected to the room and displayed on a digital display. By testing the permeability of the porous plate on the experimental platform, the relationship curves between the air flow rate and the air
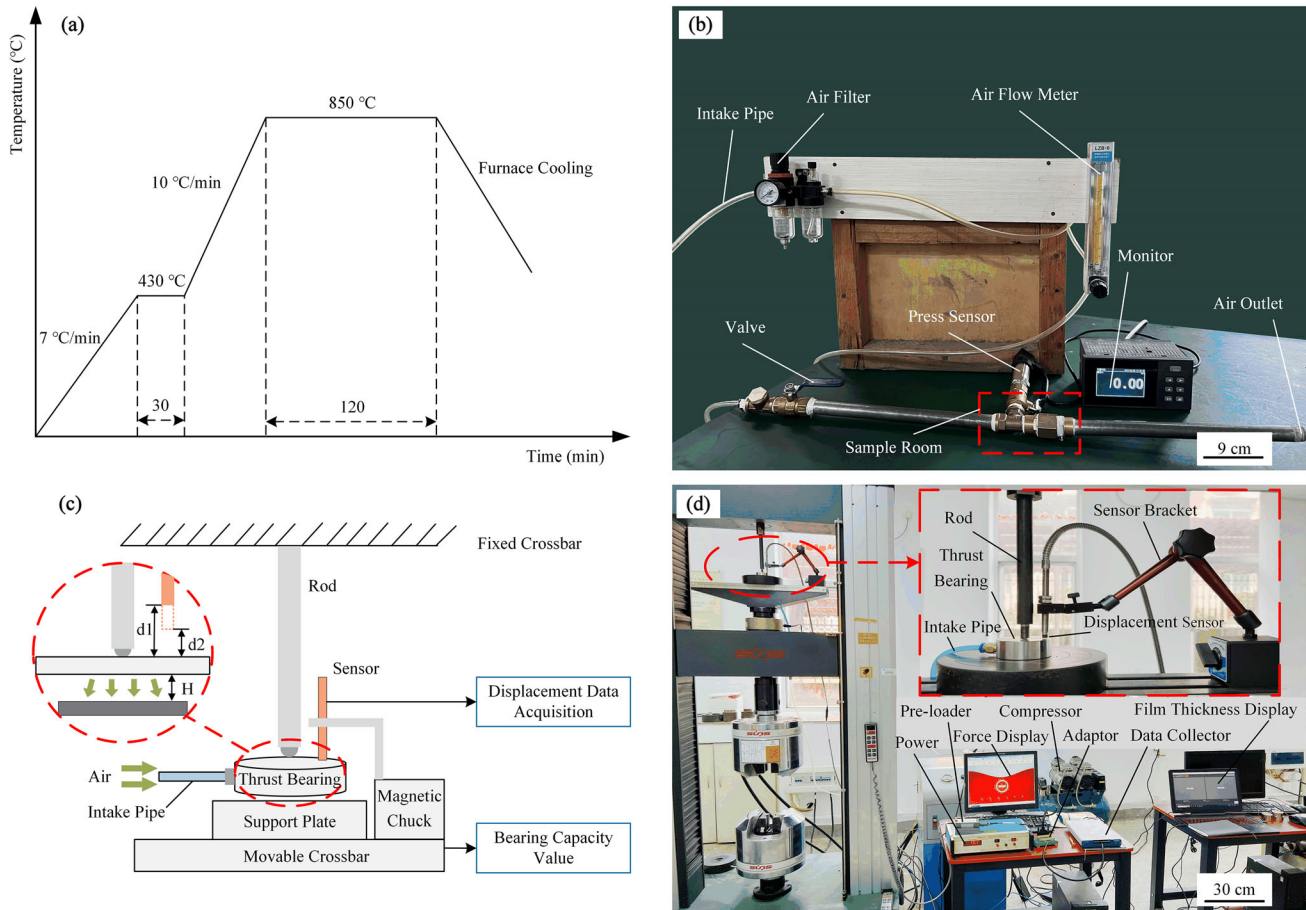
Fig. 3. (a) Sintering temperature curve, (b) air permeability testing system, (c) schematic diagram of static bearing capacity test system for porous aerostatic thrust bearing, and (d) static bearing capacity test system.

pressure difference at both ends of the sample could be obtained under different gas source pressures. The range of the airflow meter on the experimental platform was 1000 L/h, and the accuracy level of the pressure transmitter was 0.5.

Uniaxial Tensile Test

Uniaxial tensile tests were conducted on the specimens to investigate powder content's effect on the porous sheets' tensile strength. The tensile specimens were all cut by the electric discharge wire cutting method, which could ensure high machining accuracy while avoiding work hardening during machining and not damaging the surface morphology of the specimens. The specimens were taken along the porous plate's rolling direction, and the tensile specimen's gauge length was 15 mm.

Bearing Capacity Test

Based on the universal testing machine produced by SUNS Company, a bearing capacity testing platform for porous gas thrust bearings was constructed. The platform could obtain data on the gas film thickness and bearing capacity of bearings

under different experimental conditions, as shown in Fig. 3c.

The air-floating surface of the bearing was placed on the support plate, which was fixed on the movable crossbar of the testing machine. The groove at the bottom of the bearing was matched with the ball head rod. When the bearing was ventilated, the bearing was fixed on the ball head rod, and the parallelism between the air-floating surface of the bearing and the support plate was ensured. Initially, the bearing was not ventilated, and the distance between the displacement sensor head and the bearing was d_1. After the ventilation of the bearing, the distance between the head of the displacement sensor and the bearing was d_2. The difference between the two distances was the gas film thickness of the bearing H.

$$H = d_1 - d_2 \tag{3}$$

The physical image of the test platform is shown in Fig. 3d. The left side shows the universal testing machine and the built-bearing platform, and the upper right part shows an enlarged view of the platform. During the test, the microswitch was pressed on the universal testing machine to move

the movable crossbar downward. As the sensor approached the bearing, the collected d_2 value decreased, while the H value calculated in real-time by the test program written in LabVIEW increased. During the test, the universal testing machine collected the bearing capacity data corresponding to the thickness of the gas film. This way, data on a sample's gas film thickness and bearing capacity were obtained. Finally, the data were read on the film thickness and bearing capacity displays.

RESULTS AND DISCUSSION

Surface Topography Analysis

Eight different samples were selected in the article, and their parameters are given in Table I. The table shows that different mesh sizes of wire mesh and powder can be prepared through the preparation process to obtain powder/wire mesh porous plates with similar powder content and porosity. The porosity of the porous plates was distributed between 10% and 30%. The preparation process of the eight samples was the same, but the difference was that the more wire mesh sheets there were, the smaller the powder content and the larger the porosity.

The macroscopic and microscopic morphologies of the surface of Plate 1 and Plate 8 are displayed in Fig. 4. Plate 1, with a powder content of 0%, retained a purple-red metallic luster and had a smooth and flat surface in Fig. 4a. Figure 4b shows that many regularly shaped square pores were uniformly distributed on the surface of Plate 1, indicating that the wire mesh retained the pore structure and weaving form after pressing and rolling. The metal wire did not break, and the continuous metal skeleton structure positively impacted the material's mechanical properties. Figure 4c shows that the surface of Plate 8, with a powder content of 49.73%, is also flat, but the copper powder that penetrated the bottom layer can be observed. The bonding morphology of the wire mesh and powder, as well as the internal pores, can be observed in Fig. 4d. There were three primary forms of bonding: metal wire to metal wire, metal wire to powder particle, and powder particle to powder particles, marked as 1, 2, and 3 in Fig. 4d. In addition, some irregular powders became flattened after being pressed and rolled and were irregularly filled in the pores of the wire mesh, resulting in some pores being blocked.

Permeability Analysis

Figure 5a–c shows the pressure flow rate curves of each sample under different gas supply pressures of 0.2 MPa, 0.4 MPa, and 0.6 MPa. The variation curves of pressure difference with gas flow rate under different gas supply pressures were consistent, indicating that the test results were stable.

The permeability of a material is a property of its own, characterizing the ability of the fluid to pass through the material at a certain differential pressure, the magnitude of which depends on the characteristics of the fluid, pore characteristics of the porous body, porosity, shape of the pores, and thickness of the material, and is independent of the external differential pressure, the flow rate, and the flow velocity.[11] The coincidence of the pressure differential flow rate curves under different gas source pressures indicated this point.

By fitting the results of the curve with a constant free quadratic term, the quadratic polynomial coefficients of each sample could be obtained, and the viscosity permeability coefficients K_1 and inertia permeability coefficient K_2 (average) of SY-1–SY-8 also could be calculated, as shown in Table II. The higher the K_1 value was, the better the sample's permeability. According to the data in Table II, the viscous permeability coefficient K_1 of the SY-1 sample was the highest, as the copper powder content of SY-1 was 0%. The porosity was the highest when the sample thickness was close and the pore size was not filled with powder. Comparing with SY-2, SY-3, and SY-4 indicated that the smaller the mesh size of the raw material was, the better the permeability of the sample. The viscosity permeability coefficient of the 80-mesh sample increased by 142.9% compared to the 200-mesh sample because the smaller the mesh size of the raw material, the larger the wire diameter and pore size were, and the easier it was to obtain a porous plate with a large pore size. By comparing SY-2, SY-5, SY-6, SY-7, and SY-8 under conditions where the sample thickness and porosity were close, the sample's permeability decreased with the increase of powder content. When the powder content increased from 16.52% to 49.73%, the viscosity permeability coefficient of the sample decreased by 83.9%, indicating that the addition of powder could affect the porosity of the sample, thereby affecting the sample's permeability.

Tensile Testing Analysis

The tensile stress-strain curve of each sample is illustrated in Fig. 6, and each sample curve has a similar trend. The tensile strength and elongation after fracture of each sample are revealed in Table III.

Comparing SY-2, SY-3, and SY-4 showed that as the number of raw material mesh increased, the tensile strength of the specimen decreased rapidly. When the number of raw material mesh increased from 80 to 200, the tensile strength of the sample decreased from 125.5 MPa to 74.5 MPa, with a reduction ratio of 29.79%, and the elongation at break decreased from 26.40% to 16.40%. According to the existing research, the main factor affecting the tensile strength of woven wire mesh porous thin sheets was the diameter of the wire mesh itself.[17]
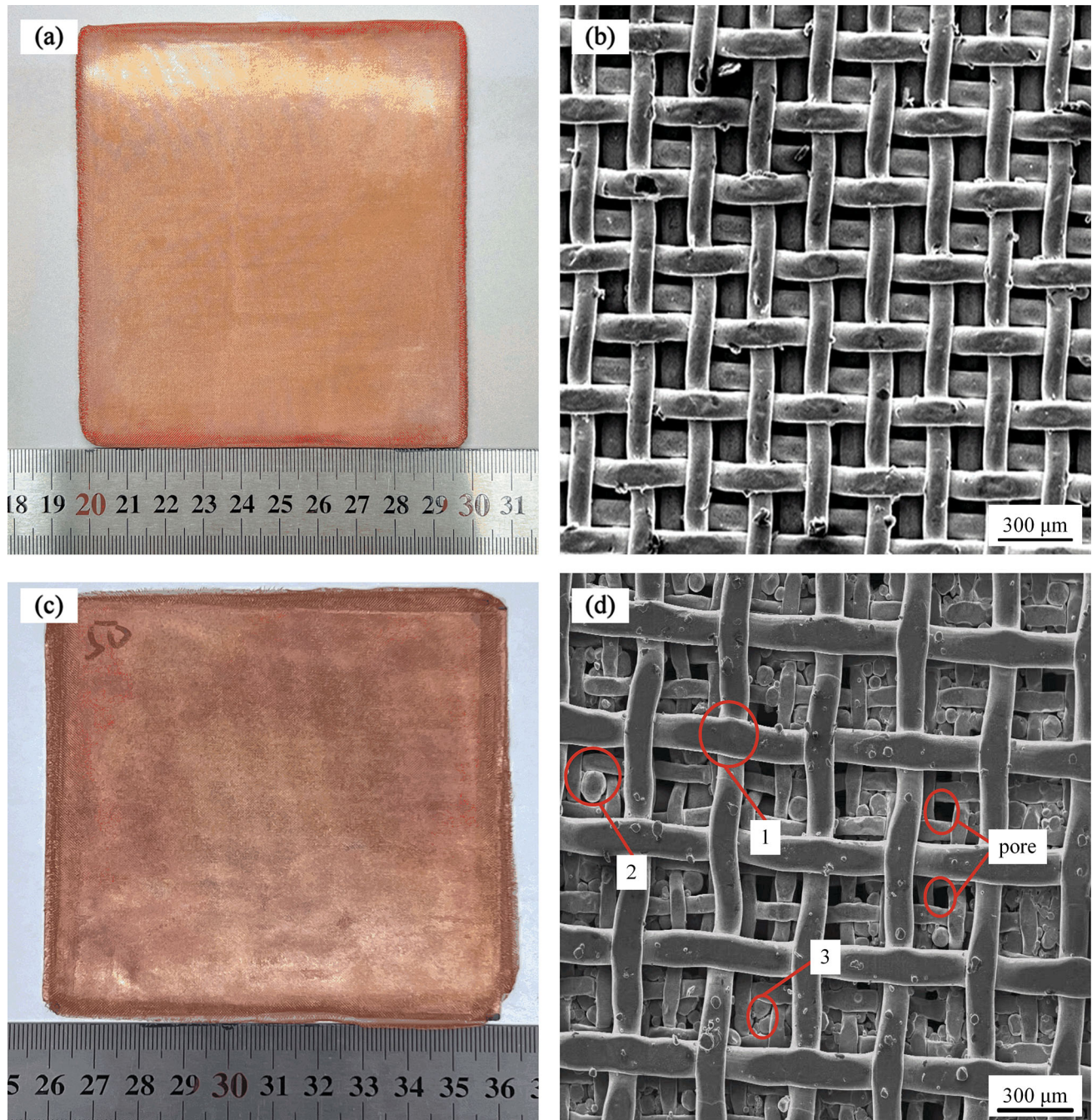
Fig. 4. Surface morphology of materials with different powder content: (a) macro-morphology and (b) surface micromorphology of plate 1, (c) macro-morphology and (d) surface micromorphology of plate 8 (Color figure online).

The theory could be extended to powder/wire mesh porous plates. A larger mesh size of wire mesh and powder meant a smaller diameter, which meant more metallurgical bonding points per unit volume. However, the metallurgical bonding between fine and fine wire and fine wire and fine powder was less reliable than that between coarse and coarse powder. Therefore, the smaller the mesh size of the wire mesh and powder, the higher the tensile strength of the composite sheet.

Comparing SY-2 and SY-8 showed that when the powder content increased from 16.52% to 49.73%, the tensile strength of the sample increased from 125.5 MPa to 208.1 MPa, an increase of 65.8%. As the powder content increased, on the one hand, the compactness per unit volume of the porous plate increased, and the porosity decreased, increasing the amount of powder and metallurgical bonding used to bear the load per unit volume. On the other hand, a larger contact area between powder and
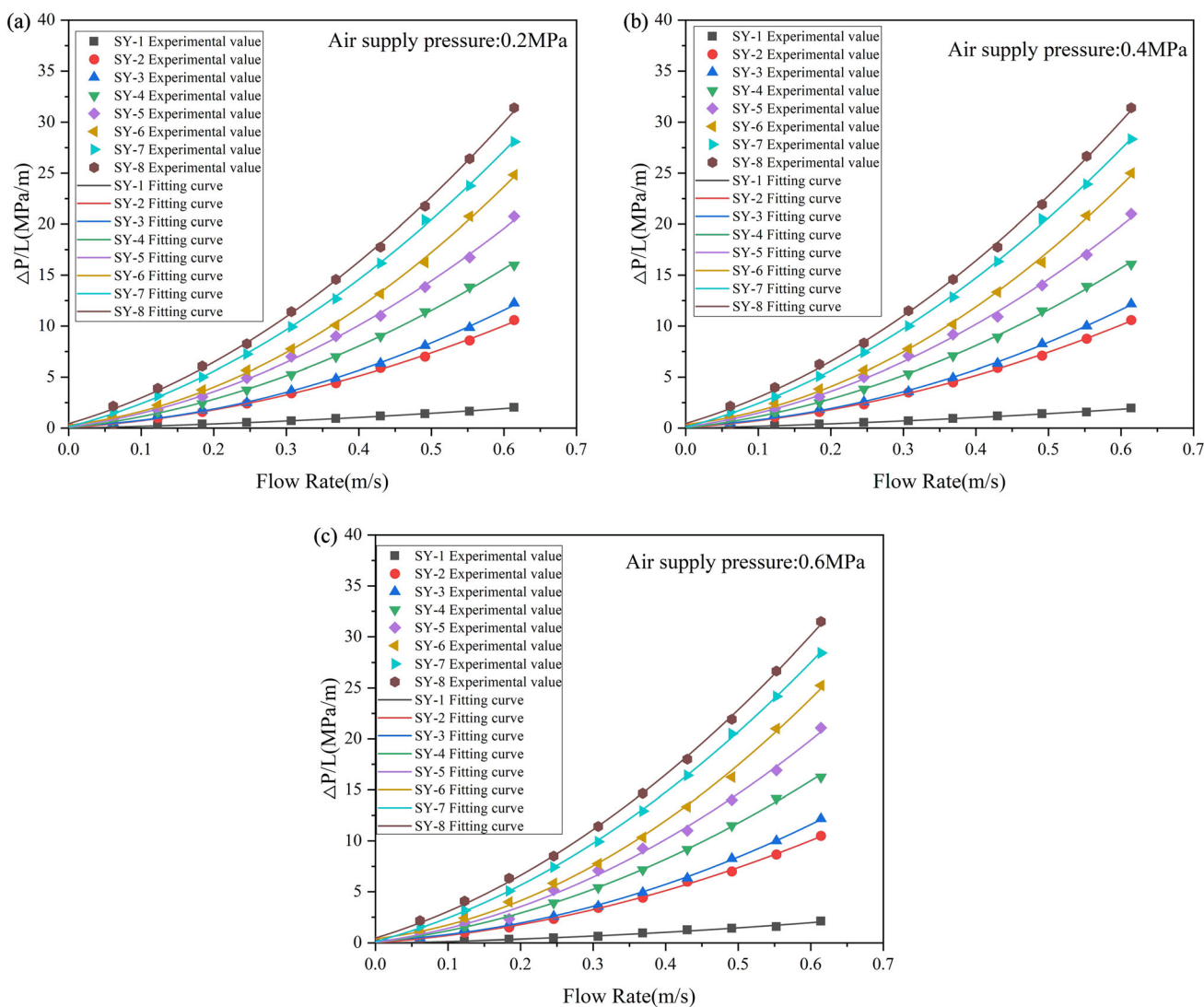
Fig. 5. Flow rate-differential pressure curves of air supply pressure of (a) 0.2 MPa, (b) 0.4 MPa, and (c) 0.6 MPa.

Table II. Permeability coefficient result of the test

Sample	Thickness (mm)	Porosity (%)	Viscous permeability coefficient $K_1 \times 10^{-11}$ (m^2)	Inertia permeability coefficient $K_2 \times 10^{-7}$ (m)
SY-1	1.21	24.31	1.005	5.005
SY-2	1.23	20.51	0.527	0.486
SY-3	1.22	20.63	0.372	0.638
SY-4	1.23	20.88	0.217	0.422
SY-5	1.24	20.04	0.211	0.247
SY-6	1.24	19.70	0.184	0.329
SY-7	1.25	19.11	0.096	0.283
SY-8	1.28	16.88	0.085	0.268

wire mesh, as well as between powder and powder, was conducive to generating larger sintering necks, making the material more resistant to damage, thereby improving the tensile mechanical properties of the material.[18]

The tensile fracture diagram of a 200-mesh powder composite porous plate is shown in Fig. 7a. Due to the high content of wire mesh and low powder content, the material bonding quality was low. Therefore, tensile fracture began where the metallurgical bonding quality was poor and then led

to fracture in other areas, ultimately leading to complete fracture of the sample.[19] The primary forms of fracture were the fracture of the metallurgical bonding surface and the necking fracture of the copper wire. Figure 7b shows several necking
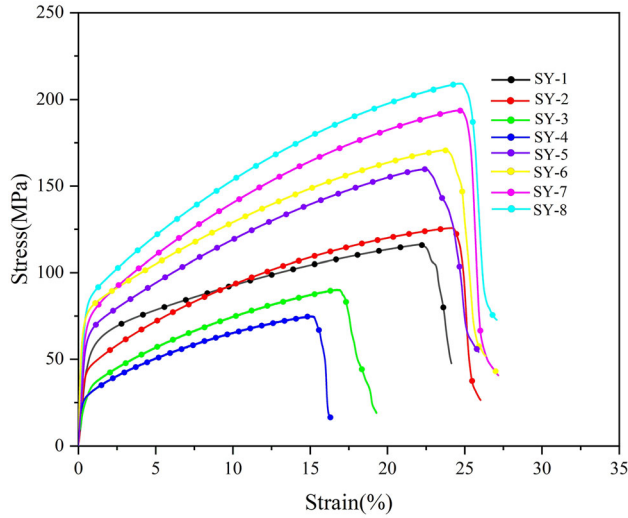

Fig. 6. Tensile stress-strain curve.

fractures and the bending deformation of the weft, which is caused by adjacent warp threads extending along the stretching direction during the stretching process.

Bearing Capacity Test Results

SY-1, SY-2, SY-5, and SY-6 were cut into porous restrictors to prepare static aerostatic thrust bearings, as shown in Fig. 8. The bearing capacity values were tested on the bearing capacity testing platform under different diameters of the restrictor, viscosity permeability coefficients, and gas supply pressures, and gas film thickness-bearing capacity curve of the bearing displayed in Fig. 9a–c was obtained. Existing research indicates that the load-carrying capacity decreases with increasing gas film thickness, and the three figures all follow this pattern.[20]

Figure 9a illustrates the bearing's gas film thickness-bearing capacity curve under different viscosity permeability coefficients when the throttle diameter is 25 mm and the gas supply pressure is 0.2 MPa. Specifically, when SY-1 was used as the throttle of the thrust bearing, and the gas film thickness was 10 μm, the bearing capacity was 210 N. In contrast, when SY-6 was used as the throttle

Table III. Result of uniaxial tensile testing

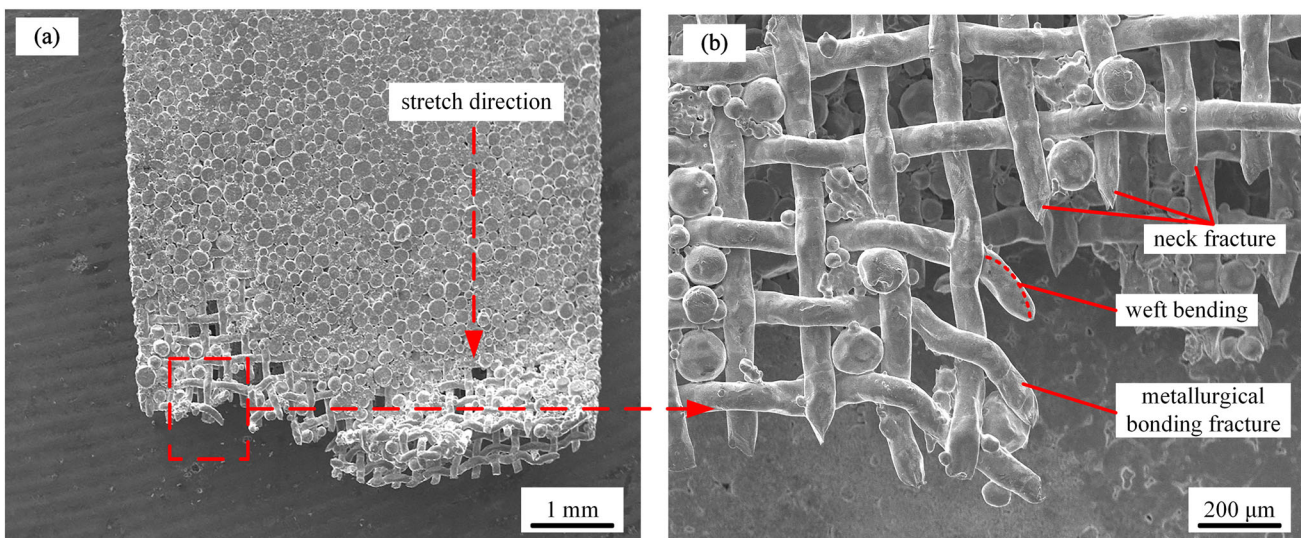| Sample	Thickness (mm)	Powder content (%)	Tensile strength (MPa)	Elongation after fracture (%)
SY-1	1.21	0	116.2	20.6
SY-2	1.23	16.52	125.5	26.4
SY-3	1.22	16.59	89.2	18.9
SY-4	1.23	16.48	74.5	16.4
SY-5	1.24	22.89	159.7	28.3
SY-6	1.24	28.36	170.6	28.6
SY-7	1.25	33.10	193.6	28.7
SY-8	1.28	49.73	208.1	29.5

Fig. 7. (a) Tensile fracture morphology of copper powder/wire mesh porous plate and (b) partially enlarged view.

of the thrust bearing, the bearing capacity was only 140 N, with a difference of 70 N between the two. The difference was not as significant as the
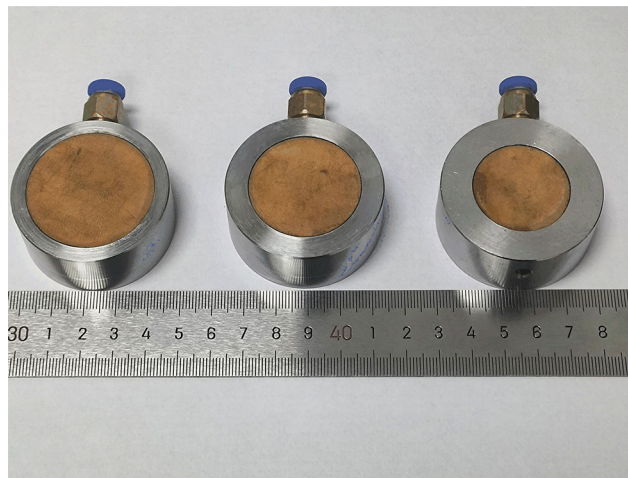

Fig. 8. Physical image of aerostatic thrust bearing.

permeability coefficient, but the former still had a 50% increase in bearing capacity compared to the latter. At the same time, the load capacity curves of other thrust bearings could also show the above pattern. It could be concluded that the thrust bearing with a more significant permeability coefficient of the porous restrictor had a better load-carrying capacity.

Figure 9b reveals the bearing's gas film thickness-bearing capacity curve under different restrictor diameters when the viscosity permeability coefficient is selected as SY-1 and the gas supply pressure is 0.2 MPa. At a gas film thickness of about 10 μm, the load capacity of a 25-mm-diameter throttle was 210 N, a 30-mm-diameter throttle was 219 N, a 35-mm-diameter throttle was 224 N, and a 40-mm-diameter throttle was 251 N. A 45-mm-diameter throttle's load capacity reached 260 N at a gas film thickness of about 13 μm. When the gas film thickness exceeded 25 μm, the gas film thickness-bearing capacity curves of the five types of bearings
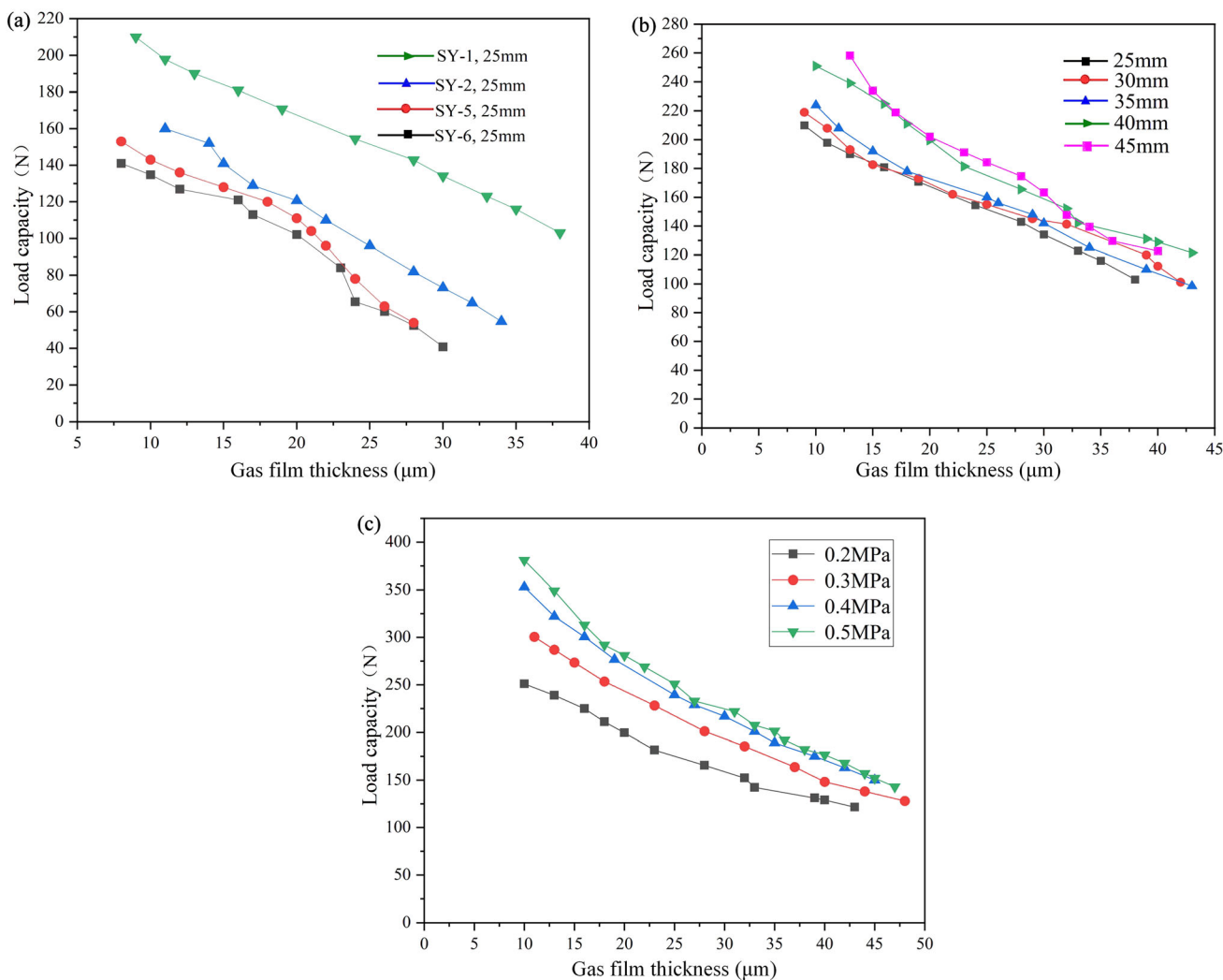

Fig. 9. Gas film thickness-bearing capacity curve of the bearing under different (a) permeability properties, (b) diameters of the restrictor, and (c) gas supply pressures.

showed an alternating up-and-down phenomenon, partly because air dissipation accelerated as the gas film thickness increased to a certain extent. As the size of the throttle increased, the air dissipation rate also accelerated. The bearing's gas film thickness-bearing capacity curve with a diameter of 40 mm was the most stable and smooth, showing the best bearing performance.

Figure 9c indicates the bearing's gas film thickness-bearing capacity curve under different gas supply pressures when the viscosity permeability coefficient is selected as SY-1 and the diameter of the throttle is 40 mm. Specifically, when the gas film thickness was 10 μm, the load-carrying capacity was 251 N, 300.5 N, 353 N, and 381 N when the gas supply pressure was 0.2 MPa, 0.3 MPa, 0.4 MPa, and 0.5 MPa, respectively. When the gas film thickness was 10 μm, the air supply pressure increased from 0.2 MPa to 0.5 MPa, and the bearing capacity increased by 130 N, with an increased ratio of 51.79%, indicating that increasing the air supply pressure could effectively improve the bearing capacity of the thrust bearing. That was because as the gas supply pressure increased, the density and collision force of gas molecules increased, increasing the gas film's stiffness and enhancing its load-bearing capacity.[14]

CONCLUSION

A copper powder/steel wire mesh porous plate was prepared using three different mesh sizes of copper powder and copper wire mesh, and its permeability and uniaxial tensile mechanical properties were tested. Finally, a throttle was fabricated from the porous plate, and the bearing capacity of the porous static aerostatic thrust bearing was tested. The following conclusions were reached:

(1) Using copper powder and copper wire mesh as raw materials, copper powder/wire mesh porous materials with porosity in the range of 10% to 30% could be prepared, in which the pore distribution was uniform, the metal skeleton was dense and continuous, and the metallurgical bonding between the metal wires could be achieved after insulation at 850°C for 2 h.

(2) The gas permeability test showed that the permeability coefficient of the copper powder/wire mesh porous plate was closely related to the mesh size and powder content of the raw material. The viscosity permeability coefficient of the porous plate decreased with the increase of the raw material's mesh size and powder content.

(3) The tensile mechanical experiment indicated that the smaller the mesh size of the raw material and the higher the powder content, the higher the tensile strength of the copper powder/wire mesh porous plate. The tensile strength of the copper powder/wire mesh porous sheet with 80 mesh size and 49.73% powder content was 208.1 MPa, which was close to the tensile strength of copper itself.

(4) The bearing capacity test of the aerostatic thrust bearings showed that the bearing capacity increased with the viscous permeability coefficient, the diameter of the porous restrictors, and the gas supply pressure. When the diameter of the throttle was 40 mm, the maximum load capacity of the aerostatic thrust bearing was 381.1 N under a supply pressure of 0.5 MPa.

CONFLICT OF INTEREST

The authors declare that they have no conflicts of interest.

REFERENCES

1. J.Y. Wang, H.P. Tang, P. Tan, and J. Zhou, *Procedia Eng.* 27, 737 (2012).
2. J. Deng and Z.Y. Zhou, *JOM* 75, 1294 (2023).
3. B. Lyu, J.Z. Chen, H.Z. Feng, C.Y. Liu, G. Ma, and M.M. Ma, *Sci. Technol. Chem. Ind.* 31, 82 (2023).
4. L.Y. Duan, Z.Y. Zhou, and B.B. Yao, *Materials.* https://doi.org/10.3390/ma11010156 (2018).
5. L.P. Lefebvre, J. Banhart, and D.C. Dunand, *Adv. Eng. Mater.* 10, 775 (2008).
6. N. Zou and Q.Z. Li, *JOM* 70, 650 (2018).
7. J. Capek and D. Vojtech, *Mater. Sci. Eng. C* 35, 21 (2014).
8. Y.J. Yi, M.J. Lee, S.J. Yun, M.H. Park, J.Y. Kim, J.W. Lee, and J.Y. Yun, *Arch. Metall. Mater.* 67, 1517 (2022).
9. Z.J. Li, T.W. Yang, Q.L. Jin, Y.H. Jiang, and R. Zhou, Rare Met. *Mater. Eng.* 43, 2609 (2014).
10. W. Liu and N. Canfield, *J. Membr. Sci.* 409–410, 113 (2012).
11. Z.Y. Zhou, H.J. Lu and J.W. Wang, *J. South China Univ. Technol. Nat. Sci* CNKI:SUN:HNLG.0.2020-04-006 (2020).
12. S. Mancin, C. Zilio, A. Cavallini, and L. Rossetto, *Int. J. Heat Mass Transfer* 53, 3121 (2010).
13. S.P. Zou, Z.P. Wan, L.S. Lu, and Y. Tang, *Materials* 9, 712 (2016).
14. C.Z. Li and Z.Y. Zhou, *Powder Technol.* https://doi.org/10.1016/J.POWTEC.2022.117205 (2022).
15. N.M. Brown and F.C. Lai, *J. Fluids Eng.* 128, 987 (2006).
16. Z.Z. Hou, Y.F. Dong, and J. Deng, *J. Filtr. Sep.* 26, 15 (2016).
17. C.Z. Li and Z.Y. Zhou, *Adv. Eng. Mater.* https://doi.org/10.1002/adem.202100585 (2021).
18. Q.B. Tan, P. Liu, C.L. Du, L.H. Wu, and G. He, *Mater. Sci. Eng. A* 527, 38 (2009).
19. S.L. Angioni, M. Meo and A, *Smart Mater. Struct.* https://doi.org/10.3390/ma11010156 (2011).
20. J.B. Zhang, D.L. Zou, N. Ta, and Z.S. Rao, *Tribol. Int.* 123, 385 (2018).